Contour Detection Based on Nonclassical Receptive Field Inhibition

Cosmin Grigorescu, *Student Member, IEEE*, Nicolai Petkov, and Michel A. Westenberg

***Abstract*—We propose a biologically motivated computational step, called nonclassical receptive field (non-CRF) inhibition, more generally surround inhibition or suppression, to improve contour detection in machine vision. Non-CRF inhibition is exhibited by 80% of the orientation-selective neurons in the primary visual cortex of monkeys and has been demonstrated to influence the visual perception of man as well. The essence of this mechanism is that the response of an edge detector in a certain point is suppressed by the responses of the operator in the region outside the area of operator support. We combine classical edge detection with two types of inhibitory mechanism, isotropic and anisotropic inhibition, both of which have counterparts in biology. For edge detection, we also use a biologically motivated method (the Gabor energy operator). The resulting operator responds strongly to isolated lines, edges, and contours, but exhibits a weaker or no response to edges that make part of texture.**

We use natural images with associated ground truth contour maps to assess the performance of the proposed operator regarding the detection of contours while suppressing texture edges. The results show that our method enhances contour detection in cluttered visual scenes more effectively than classical edge detectors used in machine vision (Canny edge detector). Therefore, the proposed operator is more useful for contour-based object recognition tasks, such as shape comparison, than traditional edge detectors, which do not distinguish between contour and texture edges. Traditional edge detection algorithms can, however, also be extended with surround suppression. Next to the advancement of contour detection in machine vision, this study contributes to the understanding of inhibitory mechanisms in biology.

***Index Terms*—Canny operator, contour detection, edge detection, Gabor energy, nonclassical receptive field inhibition, surround suppression, texture.**

I. Introduction

EDGE detection is considered a fundamental operation in image processing and computer vision. Consequently, much research has been done in this area and a considerable body of literature has been accumulated [1]–[12]. While a large number of edge detection algorithms have been proposed, research on edge detection continues to be a fertile field of activity. One of the problems with contemporary edge detectors is that they do not make a distinction between contours of objects—these are the actual primitives needed in most machine vision applications—and edges originating from textured regions. There is evidence that the human visual system makes such a difference in its early stages of visual information processing, and that isolated edges, on the one hand, and edges in a group, on the other hand, are perceived in different ways.

An important finding in the neurophysiology of the visual system of monkeys and cats, made in the beginning of the 1960s, i.e., before the development of edge detection algorithms for digital image processing, was that the majority of neurons in the primary visual cortex respond to a line or an edge of a certain orientation in a given position of the visual field. Initially, two types of orientation-selective neuron were found, one that was sensitive to the contrast polarity of lines and edges, called simple cell, and another that was not, called complex cell [13], [14]. The study of the properties of these neurons has been an active area of research [15]–[20] and, in 1981, a Nobel prize for medicine and physiology was awarded to Hubel and Wiesel who pioneered this work [21].

Later, computational models were developed aiming at simulating the function of these neurons. Simple cells can be modeled by linear filters followed by half-wave rectification [22]–[26]. Complex cells need more intricate modeling, which includes three stages: linear filtering, half-wave rectification, and subsequent local spatial summation [27]–[31]. Local energy models, in which the activities of a pair of simple cells are used to derive the activity of a complex cell, were also proposed [29], [32].

These computational models gave the basis for biologically motivated edge detection algorithms in image processing. In particular, a family of two-dimensional Gabor functions was proposed as a model of the linear filtering properties of simple cells [33], [34]. Subsequently, Gabor functions were widely used in various computer vision tasks, such as image coding and compression [35], motion analysis [36], image enhancement [37], face recognition [38], person identification based on iris pattern analysis [39], texture analysis [40]–[45], retrieval from image databases [46]–[48], and edge detection [49]–[53].

Detailed neurophysiological research revealed a considerable functional diversity in the rather broad class of orientation-selective cells. Besides the classes of simple and complex cells [13], [14], [21], [54], further classes were identified, such as end-stopped cells, originally also called hypercomplex cells [54]–[59], contour cells [60]–[62], and grating cells [63], [64]. Furthermore, the concept of a receptive field had to be reconsidered. By definition, the receptive field is the region in which an optimal stimulus elicits vigorous response from a neuron. For simple and complex cells, for instance, this is the area in which a bar or an edge of certain optimal size and orientation triggers the cell to respond. This region is presently referred to as the classical receptive field (CRF). Detailed

Manuscript received May 6, 2002; revised February 21, 2003. The associate editor coordinating the review of this manuscript and approving it for publication was Prof. Aly A. Farag.

The authors are with the Institute of Mathematics and Computing Science, University of Groningen, 9700 AV Groningen, The Netherlands (e-mail: cosmin@cs.rug.nl; petkov@cs.rug.nl; michel@cs.rug.nl).

Digital Object Identifier 10.1109/TIP.2003.814250

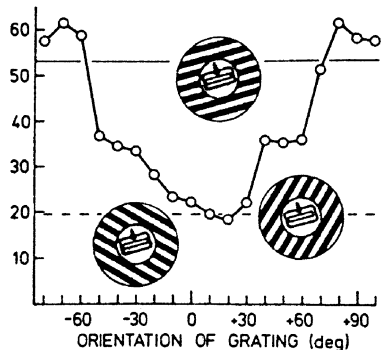

Fig. 1. Effect of orientation contrast in non-CRF inhibition [69]: the plot shows the response of a neuron to a stimulus composed of a single bar of optimal orientation in the CRF (central circle) and a grating of varying orientation outside the CRF. The inhibition by the surrounding grating is strongest when its orientation coincides with the orientation of the optimal stimulus. (Courtesy of C. Blakemore and Exp. Brain Res.).

studies have shown that once a cell is activated by a stimulus in its CRF, another, simultaneously presented stimulus outside that field can have an effect on the cell response [65], [66]. This, mostly inhibitive effect is referred to as *nonclassical receptive field (non-CRF) inhibition*; it turned out to be the rule rather than the exception, being exhibited to a different extent by 80% of the orientation-selective cells [67], [68]. Many studies focussed on the effect of orientation contrast [66], [67], [69]–[73]. Blakemore and Tobin [69], for instance, measured the response of a cell to a white bar of optimal orientation, position, and size in the presence of a grating covering the area outside the CRF. They observed an inhibitory effect caused by the grating. This effect was strongest when the grating had the same orientation as the optimal bar stimulus; in this case the response of the cell was reduced to the level of spontaneous activity. The inhibitory effect of the grating decreased with the deviation of its orientation from the optimal orientation, see Fig. 1. The dependence of the non-CRF inhibition on the relative orientation, contrast, spatial frequency, and position of the distractor stimulus was studied in [74]. In general, an orientation-selective cell with non-CRF inhibition will respond most strongly to a single bar, line, or edge in its receptive field and will show reduced response when more bars are added to the surroundings. In an extreme case, such a cell responds to an isolated bar or line, but does not respond to a system of such stimuli [64]. Such cells have actually been found by neurophysiologists: Schiller *et al.* [75], for instance, found many cells in area V1 which responded strongly to single bars and edges but did not respond to sine-wave gratings. Similar cells were encountered by Peterhans and von der Heydt [64] in experiments with bars, edges, and square-wave gratings as test stimuli. This type of cell was called the *bar cell*, referring to the preference of the cell for bars versus gratings, and a computational model was proposed for it [76].

The neurophysiological data mentioned above correlates well with the results of various psychophysical experiments, which have shown that the perception of an oriented stimulus, such as a line, can be influenced by the presence of other such stimuli (distractors) in its neighborhood. This influence can, for instance, manifest itself in an overestimation of an acute angle between

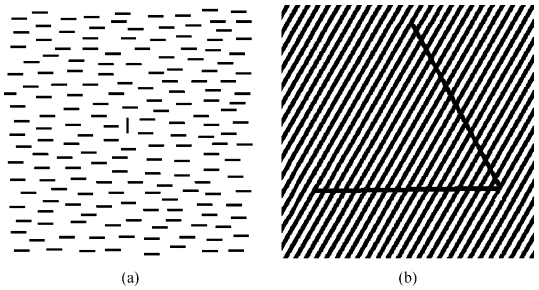

Fig. 2. (a) The pop-out effect of an oriented line segment on a background of other segments, the distractors, correlates well with the response of the neuron shown in Fig. 1 as a function of the orientation contrast: the segment pops out only if its orientation is sufficiently different from that of the background. (b) The three legs of the triangle are not perceived in the same way: the leg that is parallel to the bars of the grating is less salient than the other two legs [80].

two lines [77], or in the so-called orientation contrast pop-out effect [67], see Fig. 2(a). Fig. 2(b) illustrates the suppression of contour perception by a grating. The contour "disappears" in a grating most easily when the grating consists of elements similar to the contour. The latter effect was shown to exhibit a specific dependence on the spatial frequency of the distractor signal [78], [79].

As non-CRF inhibition seems to be a common property of biological edge detectors that determines human perception of edges and lines, we considered a more close examination of the role of this mechanism in the process of edge detection and evaluating its potential usefulness in image processing and computer vision algorithms to be worthwhile. Our main hypothesis is that this mechanism suppresses edges which make part of texture, while it does not suppress edges that belong to the contours of objects. An edge detection algorithm which employs this inhibition mechanism will thus primarily detect contours of objects, and it will not respond (sufficiently) to edges which belong to texture regions. The edge maps generated by such an edge detector will thus be more useful for contour-based object recognition tasks, such as shape comparison [81], [82], than traditional edge detectors which do not make a difference between contour and texture edges.

The paper is organized as follows. Section II describes computational models. Simple cell and complex cell models and the related Gabor and Gabor energy filters are briefly discussed, and two contour operators that employ non-CRF inhibition are introduced. In Section III, we evaluate the performance of the contour operators. A performance measure is defined, and experimental results obtained with the contour operators and the Canny edge detector are compared. Finally, we summarize the results and draw conclusions in Section IV.

II. Computational Models

A. Simple Cells and Gabor Filters

The spatial summation properties of simple cells can be modeled by a family of two-dimensional Gabor functions [83]. We use a modified parameterization to take into account restrictions found in experimental data [76], [84]. A receptive field function of such a cell, in engineering terms the impulse response,

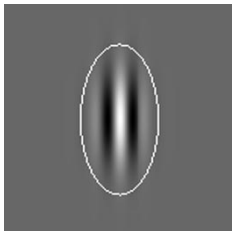

Fig. 3. Intensity map of a Gabor function, which models the receptive field profile of a simple cell. Gray levels which are lighter and darker than the background indicate zones in which the function takes positive and negative values, respectively. The bright ellipse $x^2 + (\gamma y)^2 = 4\sigma^2$ specifies the boundary of the (classical) receptive field outside which the function takes negligibly small values.

$g_{\lambda,\sigma,\theta,\varphi}(x,y), (x,y) \in \Omega \subset \mathbb{R}^2$, which is centered in the origin, is given by

$$\begin{aligned} g_{\lambda,\sigma,\theta,\varphi}(x,y) &= e^{-\frac{\tilde{x}^2+\gamma^2\tilde{y}^2}{2\sigma^2}} \cos\left(2\pi\frac{\tilde{x}}{\lambda}+\varphi\right) \\ \tilde{x} &= x\cos\theta + y\sin\theta, \\ \tilde{y} &= -x\sin\theta + y\cos\theta \end{aligned} \tag{1}$$

where $\gamma = 0.5$ is a constant, called the spatial aspect ratio, that determines the ellipticity of the receptive field. The standard deviation σ of the Gaussian factor determines the size of the receptive field. The parameter λ is the wavelength and $1/\lambda$ the spatial frequency of the cosine factor. The ratio σ/λ determines the spatial frequency bandwidth, and, therefore, the number of parallel excitatory and inhibitory stripe zones which can be observed in the receptive field, see Fig. 3. In this paper, we fix the value of this ratio to $\sigma/\lambda = 0.56$, which corresponds to a half-response bandwidth of one octave. The angle parameter θ, $\theta \in [0,\pi)$, determines the preferred orientation. The parameter φ, $\varphi \in (-\pi,\pi]$, is a phase offset that determines the symmetry of $g_{\lambda,\sigma,\theta,\varphi}(x,y)$ with respect to the origin: for $\varphi = 0$ and $\varphi = \pi$ it is symmetric (or even), and for $\varphi = -(\pi/2)$ and $\varphi = (\pi/2)$ it is antisymmetric (or odd); all other cases are asymmetric mixtures.

The response $r_{\lambda,\sigma,\theta,\varphi}(x,y)$ of a simple cell with a receptive field function $g_{\lambda,\sigma,\theta,\varphi}(x,y)$ to an input image with luminance distribution $f(x,y)$ is computed by convolution

$$\begin{aligned} r_{\lambda,\sigma,\theta,\varphi}(x,y) &= (f * g_{\lambda,\sigma,\theta,\varphi})(x,y) \\ &= \iint_{\Omega} f(u,v) g_{\lambda,\sigma,\theta,\varphi}(x-u, y-v)\mathrm{d}u\mathrm{d}v. \end{aligned} \tag{2}$$

The model used in [84] also involves thresholding and contrast normalization, but we do not need these aspects of the function of simple cells in the context of this paper. In image processing and computer vision, the filter defined by (1) and (2) is known as the (linear) Gabor filter.

B. Complex Cells and Gabor Energy Filters

The Gabor energy is related to a model of complex cells which combines the responses of a pair of simple cells with a phase difference of $(\pi/2)$ [29], [32]. The results $r_{\lambda,\sigma,\theta,0}(x,y)$ and $r_{\lambda,\sigma,\theta,-(\pi/2)}(x,y)$ of a pair of symmetric and antisymmetric filters are combined in the Gabor energy $E_{\lambda,\sigma,\theta}(x,y)$ as follows:

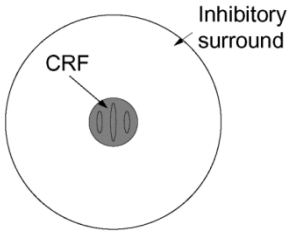

Fig. 4. Non-CRF inhibition is caused by the surroundings of the CRF, which is defined by the weighting function $w_\sigma(x,y)$, cf. (5).

$$E_{\lambda,\sigma,\theta}(x,y) = \sqrt{r^2_{\lambda,\sigma,\theta,0}(x,y) + r^2_{\lambda,\sigma,\theta,-\frac{\pi}{2}}(x,y)}. \tag{3}$$

It can be shown that the Gabor energy is equal to the square root of the local power spectrum of the image within a given orientation and spatial frequency passband [85].

In the following, we will use Gabor energy maps $E_{\lambda,\sigma,\theta_i}(x,y)$ for a number of N_θ different orientations θ_i:

$$\theta_i = \frac{(i-1)\pi}{N_\theta}, \quad i = 1,2,\ldots,N_\theta. \tag{4}$$

C. Models of Non-CRF Inhibition

We now extend the Gabor energy operator presented above with an inhibition term to qualitatively reproduce the non-CRF inhibition behavior of most orientation-selective cells. We consider two types of inhibition: i) anisotropic, in which only responses obtained for the same preferred orientation as a central response contribute to the suppression and ii) isotropic, in which all responses outside the CRF contribute to the suppression in an equal way, independently of their preferred orientations.

For a given point in the image, the inhibition term is computed in a ring-formed area surrounding the CRF centered at the concerned point, see Fig. 4. We use a normalized weighting function $w_\sigma(x,y)$ defined as follows:

$$\begin{aligned} w_\sigma(x,y) &= \frac{1}{\|H(\mathrm{DoG}_\sigma)\|_1} H\left(\mathrm{DoG}_\sigma(x,y)\right), \\ H(z) &= \begin{cases} 0, & z < 0 \\ z, & z \geq 0 \end{cases} \end{aligned} \tag{5}$$

where $\|.\|_1$ denotes the L_1 norm, the function $H(z)$ ensures that the operator has only positive response, and $\mathrm{DoG}_\sigma(x,y)$ is the following difference of Gaussian functions:[1]

$$\mathrm{DoG}_\sigma(x,y) = \frac{1}{2\pi(4\sigma)^2} e^{-\frac{x^2+y^2}{2(4\sigma)^2}} - \frac{1}{2\pi\sigma^2} e^{-\frac{x^2+y^2}{2\sigma^2}}. \tag{6}$$

1) Anisotropic Non-CRF Inhibition: We model anisotropic non-CRF inhibition by computing an inhibition term

[1]The combination of standard deviations 4σ and σ was chosen in such a way that the zero crossings of $\mathrm{DoG}_\sigma(x,y)$ are near the circle $x^2+y^2 = 4\sigma^2$. More precisely, one can take $\bar{x}^2 + (\gamma\bar{y})^2$ instead of x^2+y^2 as an argument on the right hand side of (6) with $\bar{x}$ and $\bar{y}$ according to (1). The concerned area will then have an elliptic boundary as the one shown in Fig. 3. We did not do that for reasons of simplicity and computational efficiency, and also because this did not influence the results substantially.

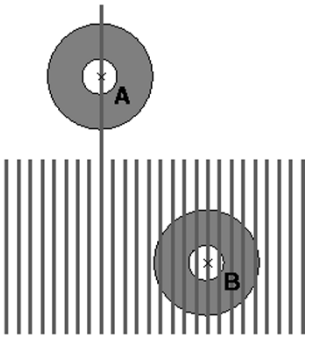

Fig. 5. Inhibition term for a given point is computed by integration over the shaded annular area surrounding that point. In a contour point, A, the inhibition term $t^A_{\lambda,\sigma,\theta_i}(x,y)$ is small. In a texture point, B, this term can become very strong.

$t^A_{\lambda,\sigma,\theta_i}(x,y)$ for each orientation θ_i as a convolution of the Gabor energy $E_{\lambda,\sigma,\theta_i}(x,y)$ with the weighting function $w_\sigma(x,y)$

$$t^A_{\lambda,\sigma,\theta_i}(x,y) = (E_{\lambda,\sigma,\theta_i} * w_\sigma)(x,y). \tag{7}$$

We now introduce a new operator $\tilde{b}^{A,\alpha}_{\lambda,\sigma,\theta_i}(x,y)$ which takes as its inputs the Gabor energy $E_{\lambda,\sigma,\theta_i}(x,y)$ and the inhibition term $t^A_{\lambda,\sigma,\theta_i}(x,y)$:

$$\tilde{b}^{A,\alpha}_{\lambda,\sigma,\theta_i}(x,y) = H\left(E_{\lambda,\sigma,\theta_i}(x,y) - \alpha t^A_{\lambda,\sigma,\theta_i}(x,y)\right) \tag{8}$$

with $H(z)$ defined as in (5). The factor α controls the strength of the inhibition of the surroundings on the Gabor energy operator.

If there is no texture in the surroundings of a given point (see point A in Fig. 5), there will be (almost) no inhibition, and the response of this operator at that point will be (almost) equal to the Gabor energy response. An edge passing through that point will be detected by this operator in the same way as it is detected by the Gabor energy operator (of appropriate orientation). However, if there are other edges in the surroundings (see point B in Fig. 5), the inhibition term $t^A_{\lambda,\sigma,\theta_i}(x,y)$ may become so strong that it cancels completely the contribution of the Gabor energy operator, resulting in a zero response.

We now construct a contour operator $b^{A,\alpha}_{\lambda,\sigma}(x,y)$ with values of maximum response of $\tilde{b}^{A,\alpha}_{\lambda,\sigma,\theta_i}(x,y)$ over all orientations

$$b^{A,\alpha}_{\lambda,\sigma}(x,y) = \max\left\{\tilde{b}^{A,\alpha}_{\lambda,\sigma,\theta_i}(x,y) | i = 1,\ldots,N_\theta\right\} \tag{9}$$

and an orientation map $\Theta^A(x,y)$ with the orientation for which this maximum response is achieved

$$\Theta^A(x,y) = \theta_k, \quad k = \arg\max\left\{\tilde{b}^{A,\alpha}_{\lambda,\sigma,\theta_i}(x,y) | i = 1,\ldots,N_\theta\right\}. \tag{10}$$

Defined in this way, the operator will respond to isolated lines, edges, and bars (of any orientation), but it will not respond to groups of such stimuli that make part of a texture grating (of the same orientation), see Fig. 6(c).

Note that, for the type of suppression modeled by (7) and (8), surround lines and edges of the same orientation as the main stimulus over the CRF will have stronger suppression effect than such stimuli of other orientations, with suppression being weakest for surround stimuli that are orthogonal to the main stimulus. For this reason, we refer to this type of modulation as *anisotropic inhibition*. This type of differential response modulation for parallel and orthogonal surround texture has been observed in 24% of a large population of orientation-selective cells in area V1 of anesthetized macaque monkeys [86]. These authors call such neurons "orientation contrast cells." In further 12% of the cells, the reverse effect of stronger suppression by an orthogonal surround texture was observed. The same authors call these latter neurons "uniform cells." Similar data were obtained for alert monkeys [67]: 32% orientation contrast cells and 6% uniform cells.

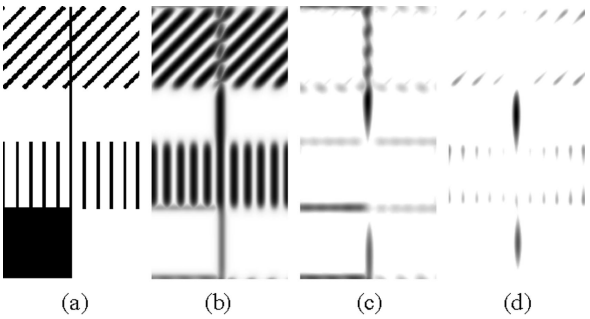

Fig. 6. (a) Synthetic input image. (b) The Gabor energy operator responds to lines and edges independently of the context, i.e., the surroundings in which these lines and edges are embedded. (c) The contour operator with anisotropic inhibition responds selectively to isolated lines and edges and lines that are surrounded by a grating of a different orientation. (d) The contour operator with isotropic inhibition responds selectively to isolated lines and edges only.

The operator defined by (8) is similar to the bar cell operator introduced in [76]. The authors of that work use as an inhibition term the response of a grating cell, which is computed in a more intricate way from the simple or complex cell responses in the surroundings. These authors introduced the term "bar cell" to emphasize the preference of the operator for bars versus gratings.

The various terms mentioned above—bar cell, orientation contrast cell, and uniform cell—focus on different aspects of the function of an orientation-selective neuron with anisotropic non-CRF inhibition.

2) Isotropic Non-CRF Inhibition: No significant difference was found in the modulation of the response to a center line stimulus by surround textures that were parallel or orthogonal to the center stimulus in 40% of the V1 cells studied in monkeys under anesthesia [86]. The authors of that paper use the term "general suppression cells" to refer to the neurons which exhibit this type of inhibition.

We refer to this type of suppression as *isotropic inhibition*, and model it by computing an inhibition term $t^I_{\lambda,\sigma}(x,y)$ that is independent of orientation. First, we construct an energy map $\widehat{E}_{\lambda,\sigma}(x,y)$ with values of maximum Gabor energy response

$$\widehat{E}_{\lambda,\sigma}(x,y) = \max\left\{E_{\lambda,\sigma,\theta_i}(x,y) | i = 1,\ldots,N_\theta\right\} \tag{11}$$

and an orientation map $\Theta^I(x,y)$ with the orientation for which these maximum responses are achieved

$$\Theta^I(x,y) = \theta_k, \quad k = \arg\max\left\{E_{\lambda,\sigma,\theta_i}(x,y) | i = 1,\ldots,N_\theta\right\}. \tag{12}$$

Now, the isotropic inhibition term $t^I_{\lambda,\sigma}(x,y)$ is computed as a convolution of the maximum energy map $\widehat{E}_{\lambda,\sigma}(x,y)$ with the weighting function $w_\sigma(x,y)$

$$t^I_{\lambda,\sigma}(x,y) = (\widehat{E}_{\lambda,\sigma} * w_\sigma)(x,y). \tag{13}$$

We now introduce the contour operator $b^{I,\alpha}_{\lambda,\sigma}(x,y)$ which takes as its inputs the maximum energy map $\widehat{E}_{\lambda,\sigma}(x,y)$ and the inhibition term $t^I_{\lambda,\sigma}(x,y)$

$$b^{I,\alpha}_{\lambda,\sigma}(x,y) = H\left(\widehat{E}_{\lambda,\sigma}(x,y) - \alpha t^I_{\lambda,\sigma}(x,y)\right) \tag{14}$$

with $H(z)$ defined as in (5). As before, the factor α controls the strength of the inhibition of the surroundings on the maximum Gabor energy term. This operator will respond to isolated lines, bars, and edges in the same way as the operator with anisotropic inhibition, but it will not respond to groups of such stimuli that make part of texture (of any orientation); see Fig. 6(d).

D. Binary Contour Map Construction

Binary contour maps are constructed by the standard procedure of nonmaxima suppression followed by hysteresis thresholding [1], [87]. From the response $b^{I,\alpha}_{\lambda,\sigma}(x,y)$ (or $b^{A,\alpha}_{\lambda,\sigma}(x,y)$) and corresponding orientation map $\Theta^I(x,y)$ (or $\Theta^A(x,y)$) that specify the local edge strength and local edge direction, respectively, nonmaxima suppression thins the edges to one-pixel wide candidate contours. The final binary contour map is computed from the candidates by hysteresis thresholding. This process involves two threshold values t_l and t_h, $t_l < t_h$. Commonly, t_h is computed as a quantile $t_h(1-p)$, where p is the minimum fraction of candidate pixels to be retained in the final contour map. We fix the low threshold value t_l to $t_l = 0.5t_h$.

Although a multitude of other post-processing methods can be found in the literature [10], [88], some of which may deliver better results than the one used here, we decided to perform the same post-processing operations as in the Canny edge detector [1] in order to simplify comparison in a later stage.

III. Performance Evaluation

Methods for evaluation of edge detector performance can be categorized as using either synthetic or natural images, with or without specified ground truth [10], [12]. When the ground truth is given, performance evaluation can be readily carried out by comparing detected edges with the ground truth edges. Although synthetic images allow precise objective definition of ground truth and seem appropriate for any performance evaluation criterion, the conclusions drawn in most of the cases are not easily extrapolated for natural scenes [89]. Additional qualitative metrics such as smoothness, continuity, thinness, which may sometimes be computed in absence of the ground truth, do not always properly reflect performance [90]. For these reasons, most of the current evaluation methods use natural image scenes with an associated ground truth specified by a human [12], [91], [92]. For a comprehensive list of performance evaluation methods for edge detection we refer to [12].

Some evaluation methods [91], [92] assess edge detector performance in the context of a well-defined task, suggesting that performance is task dependent. In this respect, some edge detectors may perform better for a specific task (e.g. structure from motion, object recognition) and worse for other tasks. Since the contour operators suppress edges in presence of surrounding texture, and retain isolated edges, we evaluate their performance on images representing objects on textured background. We selected a set of 40 images which depict either man-made objects on textured background or animals in their natural habitat; for each image, an associated ground truth binary contour map was drawn by hand.[2] Fig. 7, first and second row, presents a subset of these images together with their corresponding ground truth contour maps. Note that the ground truth maps specify *contours of objects*, not just edges.

A. Performance Measure

Let E_{GT} and B_{GT} be the set of contour pixels and background pixels of the ground truth contour image, respectively, and E_{D} and B_{D} be the set of contour pixels and background pixels of the contour image generated by an operator, respectively. The set of correctly detected contour pixels is $E = E_{\mathrm{D}} \cap E_{\mathrm{GT}}$. False negatives, i.e. ground-truth contours missed by the contour detector, are given by the set $E_{\mathrm{FN}} = E_{\mathrm{GT}} \cap B_{\mathrm{D}}$, while false positives (spurious contours) are given by the set $E_{\mathrm{FP}} = E_{\mathrm{D}} \cap B_{\mathrm{GT}}$. We define a *performance measure* of a contour detector as

$$P = \frac{\mathrm{card}(E)}{\mathrm{card}(E) + \mathrm{card}\,(E_{\mathrm{FP}}) + \mathrm{card}\,(E_{\mathrm{FN}})} \tag{15}$$

in which card (X) denotes the number of elements of the set X.

The performance measure P is a scalar taking values in the interval [0,1]. If all true contour pixels are correctly detected and no background pixels are falsely detected as contour pixels, then $P = 1$. For all other cases, the performance measure takes sub-unitary values, being closer to zero as more edge pixels are falsely detected and/or missed by the contour operator.

Since contours cannot always be detected at exact integer image coordinates, we consider that a contour pixel is correctly detected if a corresponding ground truth contour pixel is present in a 5×5 square neighborhood centered at the respective pixel coordinates. The false negatives and false positives are determined by eliminating those pixels which are correctly detected from the ground truth contours and detected contours, respectively.

Other measures, often used for evaluating segmentation results [93], cast the performance into a classification error computed for a two class assignment problem. In this case, the error can be expressed as the number of misclassified contour pixels (i.e., false positives and false negatives) divided by the total number of pixels in the image. Though intuitively appealing, such a measure has the drawback that it does not scale linearly with the number of detected contour pixels (e.g., an increase by the same number of misclassified pixels for a contour image which has 10 contour pixels delivers the same performance as an image consisting of 1000 contour pixels, assuming that both images have the same size). In contrast, the measure defined by

[2]The images and associated ground truths are available at (http://www.cs.rug.nl/~imaging).

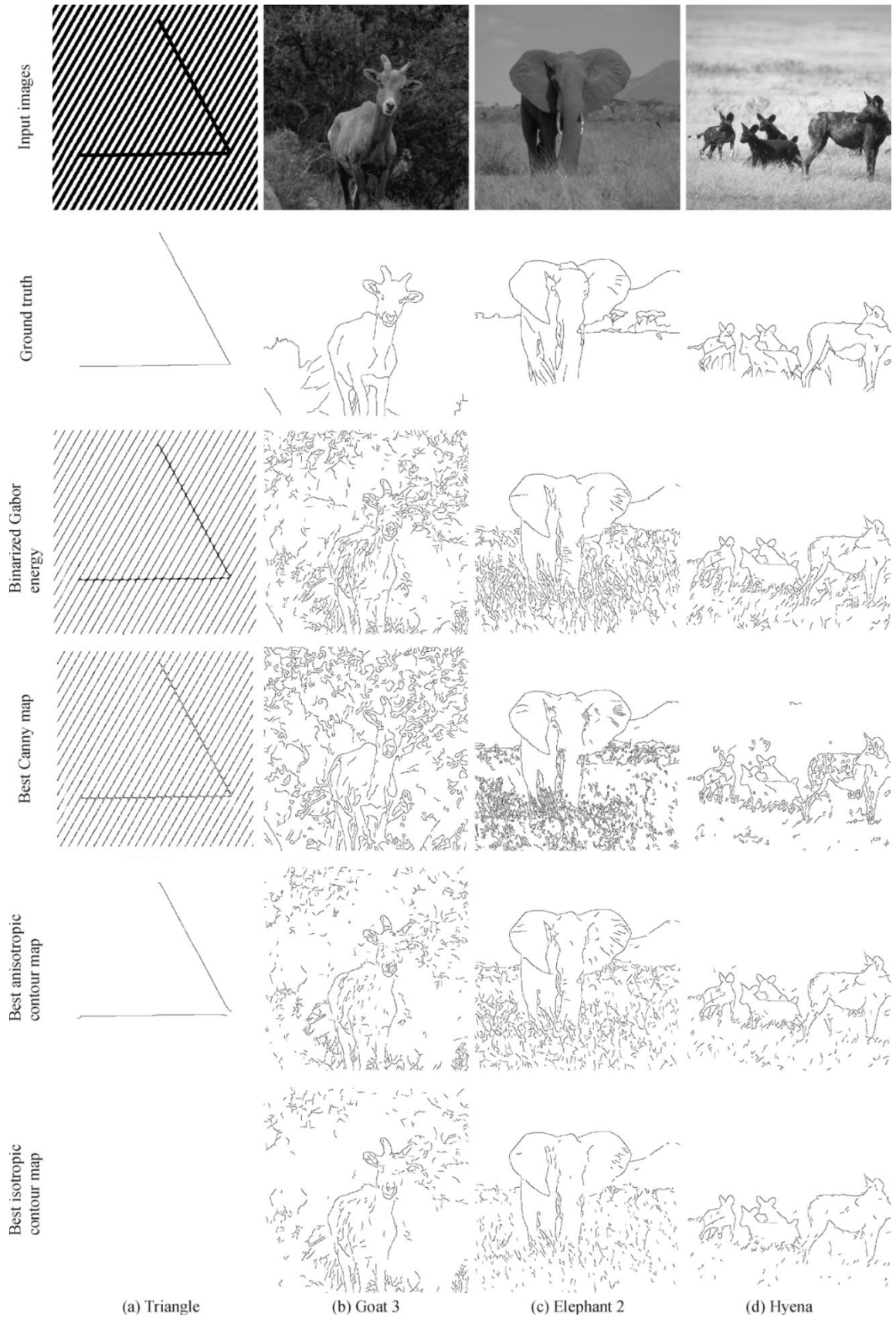

Fig. 7. One synthetic image and three natural scenes with objects on textured backgrounds (first row), their corresponding ground truth contour maps (second row), the binarized Gabor energy maps (third row), the best edge maps obtained with the Canny edge detector (fourth row), the best contour maps obtained with the anisotropic contour operator (fifth row), and the best contour maps obtained with the isotropic contour operator (last row).

(15) reflects an increase/decrease in the number of misclassified contour pixels versus the number of detected contour pixels proportionally.

B. Experimental Results

We compare the performances of the two contour operators defined above with the performance of the Gabor energy operator as defined in (3), i.e., without inhibition, and the Canny edge detector.

The Canny edge detection operator [1] consists of a gradient computation for each pixel of the image, and construction of a binary edge map by post-processing with nonmaxima suppression and hysteresis thresholding. The gradient is computed using a scale-dependent differential geometry operator. We applied the same type of post-processing for binarization to the Gabor energy operator.

The two parameters of the Canny edge detector are σ, the standard deviation of a Gaussian smoothing kernel, and p, the minimum fraction of edge pixels that have to be retained in the final edge map. The same parameters are used for the Gabor energy operator, where the parameter σ denotes the standard deviation of the Gaussian factor of the concerned Gabor function. The contour operators have an additional parameter, α, which is the texture inhibition factor. For the Canny edge detector, we used eight scales, $\sigma \in \{1.0, 1.2, 1.4, 1.6, 1.8, 2.0, 2.2, 2.4\}$. For the contour operators we used four scales covering the same domain, $\sigma \in \{1.2, 1.6, 2.0, 2.4\}$ and two texture attenuation factors, $\alpha \in \{1.0, 1.2\}$. For all methods, we applied five high hysteresis threshold values based on the fraction p of the candidate pixels that should be retained in the contour edge map, with $p \in \{0.5, 0.4, 0.3, 0.2, 0.1\}$. This results in 40 parameter combinations for each of the methods. For the Gabor energy and contour operators, we used 12 orientations, $N_\theta = 12$.

The maps with best contour detection performance for a small selection of our test images are shown in Fig. 7. The first and second row show the input images and the ground truth images, respectively, the third row shows the responses of the binarized output of the Gabor energy operator, and the fourth, fifth, and sixth rows show the results for the Canny edge detector, the contour operator with anisotropic inhibition and with isotropic inhibition, respectively. For a better illustration, we also computed the fraction of false positives e_{FP} as the ratio between the number of false positives and the number of correctly detected contour pixels ($e_{\mathrm{FP}} = \mathrm{card}(E_{\mathrm{FP}})/\mathrm{card}(E)$), and the fraction of false negatives e_{FN} as the ratio between the number of false negatives and the number of ground truth contour pixels ($e_{\mathrm{FN}} = \mathrm{card}(E_{\mathrm{FN}})/\mathrm{card}(E_{\mathrm{GT}})$). The performance measures, parameters, and fractions of false positives and false negatives are listed in Table I.

The results show that the contour operator indeed suppresses edges in the presence of surrounding texture for both anisotropic and isotropic inhibition. The synthetic image presented in the first column of Fig. 7 is an interesting special case. Our perceptual interpretation of the image, two lines superimposed on a grating, is paired by the response of the contour operator with anisotropic inhibition only. The other operators—the Gabor energy operator, Canny, and the contour operator with isotropic inhibition—do not deliver results matched by perception.

TABLE I
OPERATOR PARAMETERS, ERRORS, AND PERFORMANCES FOR THE IMAGES PRESENTED IN FIG. 7

	σ	p	α	e_{FP}	e_{FN}	P
Triangle						
Gabor energy	7.0	0.5		0.93	0.00	0.04
Canny	3.0	0.5		0.95	0.00	0.04
Anisotropic	7.0	0.5	2.0	0.02	0.06	0.91
Isotropic	7.0	0.5	2.0	0.00	1.00	0.00
Goat 3						
Gabor energy	2.0	0.1		0.72	0.38	0.25
Canny	2.4	0.1		0.83	0.55	0.14
Anisotropic	2.4	0.1	1.2	0.36	0.60	0.32
Isotropic	2.0	0.1	1.0	0.46	0.51	0.34
Elephant 2						
Gabor energy	2.0	0.1		0.59	0.36	0.32
Canny	2.4	0.1		0.71	0.50	0.23
Anisotropic	2.4	0.1	1.2	0.36	0.45	0.40
Isotropic	2.0	0.1	1.0	0.31	0.49	0.42
Hyena						
Gabor energy	2.0	0.1		0.52	0.32	0.39
Canny	2.2	0.1		0.59	0.50	0.28
Anisotropic	2.4	0.1	1.2	0.37	0.25	0.51
Isotropic	2.0	0.1	1.0	0.22	0.35	0.55

The second (Goat 3) and last column (Hyena) are very good examples of the texture suppression behavior of the contour operators. The example in the second column shows also that the Canny edge map contains so many spurious edges that it is hard to distinguish the contours of the object. In contrast, distinguishing the object contours in the output of the contour operators can be done without difficulty. The performance measure is consistently higher for the contour operators, and this is mostly due to a reduced percentage of false positives. This is in agreement with the proposed model of non-CRF inhibition: edges resulting from a texture background (false positives) are suppressed, while object contours are retained.

Fig. 8 shows comparative statistical box-and-whisker plots for ten of the images used in our experiments. The plots reveal a consistent better performance of the contour operators. In all cases, the best performance (the top end of a whisker) is higher in comparison to the best performance of the Canny edge detector and the Gabor energy operator, and, in most of the cases, the isotropic inhibition gives the most effective results.

IV. DISCUSSION

The models of non-CRF inhibition we use in this study are simple and straightforward. In the anisotropic inhibition model, the response of an orientation- and scale-specific operator in a given position is suppressed by the responses of the same operator in other positions. In the isotropic inhibition model, suppression is caused also by activity in channels responsible for other orientations. Our models make use of a single parameter α that is the coefficient with which the inhibition term is taken into account. The value of this parameter can be determined in an optimization problem derived from a specific goal, e.g., maximization of the performance of the operator for a certain set of images. One can think of more intricate or general inhibition models, such as the division normalization proposed in [94],

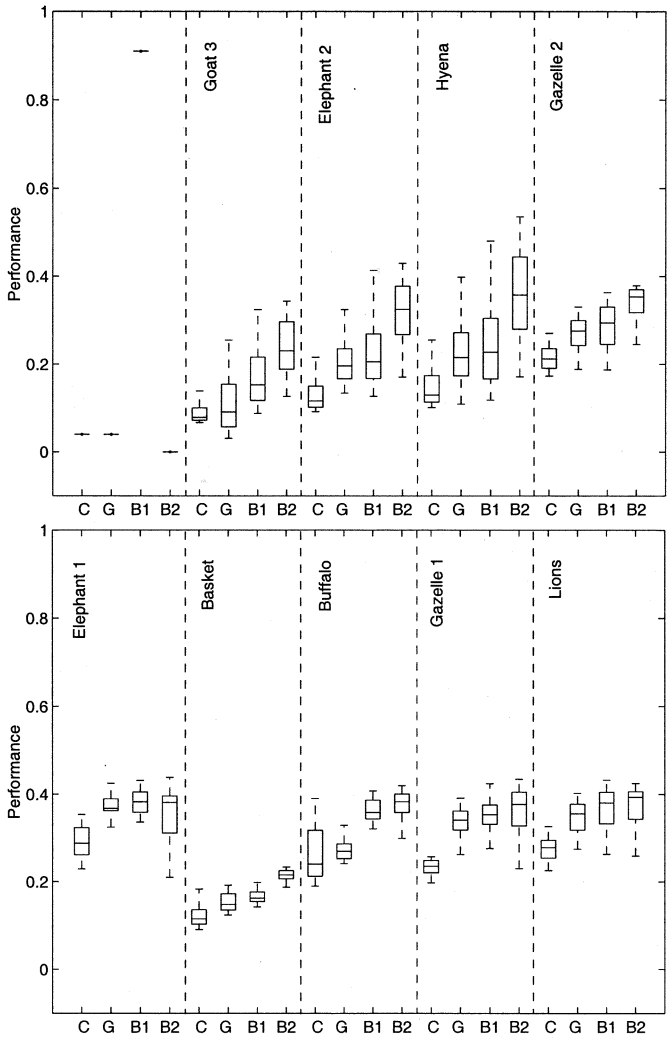

Fig. 8. Box-and-whisker plots of the performance of the Canny edge detector (denoted by C), the Gabor energy operator (denoted by G), the contour operator with anisotropic inhibition (denoted by B1) and isotropic inhibition (denoted by B2) for ten of the test images.

where the inhibition weights of the responses of all orientation and scale channels and all positions are not fixed in advance but are determined such that mutual dependencies between the ultimate responses are minimized.

Inhibition mechanisms have been applied previously to biologically motivated edge detectors in order to improve certain aspects of their function. A symmetric Gabor filter, will, for instance, respond not only along a line but will also give a flanking response alongside the line at a certain distance from it. Similarly, the largest response of an antisymmetric Gabor filter to a line will be displaced from the line. (These issues do not arise with the Gabor-energy filter.) In [50] and [95]–[97], various inhibition mechanisms have been proposed to remove these flanking responses. These works differ from the current work in two major aspects. First, the inhibition mechanisms act within the CRF. Second, the purpose of the inhibition is quite different: it deals with the removal of flanking responses, rather than with the suppression of texture edges.

The inhibitory mechanisms presented in this paper can be applied as an additional processing step to most edge detectors used in image processing. The role of a CRF is taken over by the area of essential support of the corresponding edge detector, e.g. the circular area which gives rise to 95% of the norm of a Gaussian used in a Canny operator. The surround is defined as the region outside the area of essential support. In this case, it would be more appropriate to more generally speak of *surround inhibition* or *surround suppression*. For instance, isotropic inhibition can easily be added to the Canny edge detector as an intermediate step between the gradient computation and the edge thinning and binarization. The inhibition term is computed by convolving the gradient magnitude field with the function $w_\sigma(x, y)$. With this modification, the Canny algorithm becomes essentially very similar to the contour operator with isotropic inhibition presented above: the only difference is the way in which the edge strength computation is done, by a scale-specific differential geometry operator (in the Canny algorithm) versus a multichannel bank of orientation-specific Gabor energy filters (in the case of the contour operator). The anisotropic inhibition, very effective when the background consists of oriented texture, can also be incorporated, while less directly, as a computational step into the Canny algorithm and other similar algorithms which operate on a gradient magnitude and orientation map. The inhibition step may be expected to improve contour detection performance when images contain objects of interest on a textured or cluttered background.

The non-CRF inhibition algorithms presented in this paper treat different classes of edges and lines in different ways: single contour lines and edges, on one hand, being considered as nontexture features, are not affected by the inhibition, while groups of lines and edges, on the other hand, viewed as texture features, are suppressed. As already noted in the introduction, this different treatment correlates well with human visual perception. For instance, while the contours of a single leaf of a tree on a plain background are to be seen as nontexture features, the same contours can occur as texture features when they appear in a foliage image together with the contours of many other leaves. The emergence of a separate linguistic entity, the word "texture," for a group of edges indicates a semantic difference associated with the context in which an edge appears: stand-alone as a contour of an object versus in a group of similar edges forming texture. In a similar way, separate entities have evolved in language to indicate a semantic, contextual difference between a single *tree* and a collection of trees, a *forest*.

It was suggested by Nothdurft *et al.* [86] that non-CRF inhibition may play a certain role in texture segmentation by generating sensitivity to (texture) feature contrast. Our computational models supports this assumption. The anisotropic surround inhibition operator (8), for instance, will respond more strongly at the boundary between two textures of different preferred orientations than inside uniform texture regions. Both the isotropic (14) and the anisotropic (8) operator will respond more strongly at the boundary between two textures of different frequency spectra than inside these textures. Next to this role of non-CRF inhibition, we think that the main biological utility of non-CRF inhibition is the separation of contour from texture information and the mediation of object contours to higher cortical areas as proposed previously in [76], [98]. Indeed, while non-CRF inhibition scarcely influences the responses to isolated contours,

i.e., contours that are not embedded in texture, it strongly reduces the responses to texture. The biologically (in our view) most important effect of this neural mechanism might thus be that of contour (versus texture) detection.

In summary, in this work we have shown that non-CRF inhibition, more generally surround inhibition, is a useful computational mechanism that substantially improves contour detection.

REFERENCES

[1] J. F. Canny, "A computational approach to edge detection," *IEEE Trans. Pattern Anal. Machine Intell.*, vol. PAMI-8, no. 6, pp. 679–698, 1986.

[2] F. Bergholm, "Edge focusing," *IEEE Trans. Pattern Anal. Machine Intell.*, vol. PAMI-9, pp. 726–741, 1987.

[3] S. Sarkar and K. Bowyer, "Optimal infinite impulse response zero-crossing based edge detection," in *Comput. Vis., Graph. Image Process.*, vol. 54, 1991, pp. 224–243.

[4] C. A. Rothwell, J. L. Mundy, W. Hoffman, and V. D. Nguyen, "Driving vision by topology," in *Proc. Int. Symp. Computer Vision*, Coral Gables, FL, 1995, pp. 395–400.

[5] L. Iverson and S. W. Zucker, "Logical/linear operators for image curves," *IEEE Trans. Pattern Anal. Machine Intell.*, vol. 17, no. 10, pp. 982–996, 1995.

[6] S. M. Smith and J. M. Brady, "SUSAN—a new approach to low level image processing," *Int. J. Comput. Vis.*, vol. 23, no. 1, pp. 45–78, 1997.

[7] M. Tabb and N. Ahuja, "Multiscale image segmentation by integrated edge and region detection," *IEEE Trans. Image Processing*, vol. 6, pp. 642–655, May 1997.

[8] J. C. Bezdek, R. Chandrasekhar, and Y. Attikiouzel, "A geometric approach to edge detection," *IEEE Trans. Fuzzy Syst.*, vol. 6, no. 1, pp. 52–75, 1998.

[9] M. J. Black, G. Sapiro, D. Marimont, and D. Heeger, "Robust anisotropic diffusion," *IEEE Trans. Image Processing*, vol. 7, pp. 421–432, Mar. 1998.

[10] S. Ando, "Image field categorization and edge/corner detection from gradient covariance," *IEEE Trans. Pattern Anal. Machine Intell.*, vol. 22, no. 2, pp. 179–190, 2000.

[11] P. Meer and B. Georgescu, "Edge detection with embedded confidence," *IEEE Trans. Pattern Anal. Machine Intell.*, vol. 23, pp. 1351–1365, Dec. 2001.

[12] K. Bowyer, C. Kranenburg, and A. Dougherty, "Edge detector evaluation using empirical ROC curves," *Comput. Vis. Image Understand.*, vol. 84, no. 1, pp. 77–103, 2001.

[13] D. H. Hubel and T. N. Wiesel, "Receptive fields, binocular interaction, and functional architecture in the cat's visual cortex," *J. Physiol. (Lond.)*, vol. 160, pp. 106–154, 1962.

[14] ——, "Sequence regularity and geometry of orientation columns in the monkey striate cortex," *J. Comput. Neurol.*, vol. 158, pp. 267–293, 1974.

[15] D. G. Albrecht, R. L. De Valois, and L. G. Thorell, "Visual cortical neurons: are bars or gratings the optimal stimuli?," *Science*, vol. 207, pp. 88–90, 1980.

[16] R. L. De Valois, D. G. Albrecht, and L. G. Thorell, "Cortical cells: bar and edge detectors, or spatial frequency filters," in *Frontiers of Visual Science*, S. J. Cool and E. L. Smith III, Eds. New York: Springer-Verlag, 1978.

[17] K. K. De Valois, R. L. De Valois, and E. W. Yund, "Responses of striate cortical cells to grating and checkerboard patterns," *J. Physiol. (Lond.)*, vol. 291, pp. 483–505, 1979.

[18] I. D. G. Macleod and A. Rosenfeld, "The visibility of gratings: spatial frequency channels or bar-detecting units?," *Vis. Res.*, vol. 14, pp. 909–915, 1974.

[19] C. W. Tyler, "Selectivity for spatial frequency and bar width in cat visual cortex," *Vis. Res.*, vol. 18, pp. 121–122, 1978.

[20] R. von der Heydt, "Approaches to visual cortical function," *Rev. Physiol., Biochem., Pharmacol.*, vol. 108, pp. 69–150, 1987.

[21] D. H. Hubel, "Explorations of the primary visual cortex, 1955–1978," *Nature*, vol. 299, pp. 515–524, 1982.

[22] B. W. Andrews and D. A. Pollen, "Relationship between spatial frequency selectivity and receptive field profile of simple cells," *J. Physiol. (Lond.)*, vol. 287, pp. 163–176, 1979.

[23] V. D. Glezer, T. A. Tscherbach, V. E. Gauselman, and V. M. Bondarko, "Linear and non-linear properties of simple and complex receptive fields in area 17 of the cat visual cortex," *Biol. Cybern.*, vol. 37, pp. 195–208, 1980.

[24] J. J. Kulikowski and P. O. Bishop, "Fourier analysis and spatial representation in the visual cortex," *Experientia*, vol. 37, pp. 160–163, 1981.

[25] L. Maffei, C. Morrone, M. Pirchio, and G. Sandini, "Responses of visual cortical cells to periodic and nonperiodic stimuli," *J. Physiol. (Lond.)*, vol. 296, pp. 27–47, 1979.

[26] J. A. Movshon, I. D. Thompson, and D. J. Tolhurst, "Spatial summation in the receptive fields of simple cells in the cat's striate cortex," *J. Physiol. (Lond.)*, vol. 283, pp. 53–77, 1978.

[27] ——, "Receptive field organisation of complex cells in the cat's striate cortex," *J. Physiol. (Lond.)*, vol. 283, pp. 79–99, 1978.

[28] H. Spitzer and S. Hochstein, "A complex cell receptive field model," *J. Neurophysiol.*, vol. 53, pp. 1266–1286, 1985.

[29] M. C. Morrone and D. C. Burr, "Feature detection in human vision: a phase-dependent energy model," in *Proc. R. Soc. Lond. B*, vol. 235, 1988, pp. 221–245.

[30] R. Shapley, T. Caelli, M. Morgan, and I. Rentschler, "Computational theories of visual perception," in *Visual Perception: The Neurophysiological Foundations*, L. Spillmann and J. S. Werner, Eds. New York: Academic, 1990, pp. 417–448.

[31] R. G. Szulborski and L. A. Palmer, "The two-dimensional spatial structure of nonlinear subunits in the receptive fields of complex cells," *Vis. Res.*, vol. 30, pp. 249–254, 1990.

[32] E. H. Adelson and J. R. Bergen, "Spatio-temporal energy models for the perception of motion," *J. Opt. Soc. Amer. A*, vol. 2, pp. 284–299, 1985.

[33] J. G. Daugman, "Uncertainty relations for resolution in space, spatial frequency, and orientation optimized by two-dimensional visual cortical filters," *J. Opt. Soc. Amer. A*, vol. 2, pp. 1160–1169, 1985.

[34] J. P. Jones and L. A. Palmer, "An evaluation of the two-dimensional Gabor filter model of simple receptive fields in cat striate cortex," *J. Neurophysiol.*, vol. 58, pp. 1233–1258, 1987.

[35] J. G. Daugman, "Complete discrete 2-D Gabor transforms by neural networks for image analysis and compression," *IEEE Trans. Acoust., Speech, Signal Processing*, vol. 36, no. 7, pp. 1169–1179, 1988.

[36] D. J. Heeger, "Model for extraction of image flow," *J. Opt. Soc. Amer. A*, vol. 4, pp. 1455–1471, 1987.

[37] G. Cristóbal and R. Navarro, "Space and frequency variant image enhancement based on Gabor representation," *Pattern Recognit. Lett.*, vol. 15, pp. 273–277, 1994.

[38] B. S. Manjunath, C. Shekhar, and R. Chellappa, "A new approach to image feature detection with applications," *Pattern Recognit.*, vol. 29, no. 4, pp. 627–640, 1996.

[39] J. G. Daugman, "High confidence visual recognition of persons by a test of statistical independence," *IEEE Trans. Pattern Anal. Machine Intell.*, vol. 15, no. 11, pp. 1148–1161, 1993.

[40] M. R. Turner, "Texture discrimination by Gabor functions," *Biol. Cybern.*, vol. 55, pp. 71–82, 1986.

[41] I. Fogel and D. Sagi, "Gabor filters as texture discriminator," *Biol. Cybern.*, vol. 61, pp. 103–113, 1989.

[42] J. R. Bergen and M. S. Landy, "Computational modeling of visual texture segregation," in *Computational Models of Visual Processing*, M S. Landy and J. A. Movshon, Eds. Cambridge, MA: MIT Press, 1991, pp. 253–271.

[43] A. C. Bovik, "Analysis of multichannel narrowband filters for image texture segmentation," *IEEE Trans. Signal Processing*, vol. 39, no. 9, pp. 2025–2043, 1991.

[44] A. K. Jain and F. Farrokhnia, "Unsupervised texture segmentation using Gabor filters," *Pattern Recognit.*, vol. 24, no. 12, pp. 1167–1186, 1991.

[45] T. N. Tan, "Texture edge detection by modeling visual cortical channels," *Pattern Recognit.*, vol. 28, no. 9, pp. 1283–1298, 1995.

[46] W. Y. Ma, "NETRA: A Toolbox for Navigating Large Image Databases," Ph.D. dissertation, Univ. of California, Santa Barbara, 1997.

[47] B. S. Manjunath and W. Y. Ma, "Texture features for browsing and retrieval of image data," *IEEE Trans. Pattern Anal. Machine Intell.*, vol. 18, no. 8, pp. 837–842, 1996.

[48] B. S. Manjunath, P. Wu, S. Newsam, and H. D. Shin, "A texture descriptor for browsing and similarity retrieval," in *Sign. Process.: Image Commun.*, vol. 16, 2000, pp. 33–43.

[49] M. C. Morrone and R. A. Owens, "Feature detection from local energy," *Pattern Recognit. Lett.*, vol. 6, pp. 303–313, 1987.

[50] F. Heitger, "Feature Detection Using Suppression and Enhancement," Communication Technology Laboratory, Swiss Federal Inst. Technol., Lausanne, Tech. Rep. TR-163, 1995.

[51] L. Rosenthaler, F. Heitger, O. Kübler, and R. von der Heydt, "Detection of general edges and keypoints," in *Proc. Eur. Conf. Computer Vision (ECCV'92)*, G. Sandini, Ed., 1992, pp. 78–86.

[52] R. Mehrotra, K. R. Namuduri, and N. Ranganathan, "Gabor filter-based edge detection," *Pattern Recognit.*, vol. 25, no. 12, pp. 1479–1494, 1992.

[53] P. Kovesi, "Image features from phase congruency," *J. Comput. Vis. Res.*, vol. 1, no. 3, pp. 2–27, 1999.

[54] D. H. Hubel and T. N. Wiesel, "Receptive fields and functional architecture of monkey striate cortex," *J. Physiol. (Lond.)*, vol. 195, pp. 215–243, 1968.
[55] E. Peterhans and R. von der Heydt, "The role of end-stopped receptive fields in contour perception," in *New Frontiers in Brain Research Proc. 15th Goettingen Neurobiology Conf.*, N. Elsner and O. Creutzfeld, Eds., 1987, p. 29.
[56] A. Dobbins, S. W. Zucker, and M. S. Cynader, "Endstopped neurons in the visual cortex as a substrate for calculating curvature," *Nature*, vol. 329, pp. 438–441, 1987.
[57] D. H. Hubel and T. N. Wiesel, "Receptive fields and functional architecture in two non-striate visual areas (18 and 19) of the cat," *J. Physiol. (Lond.)*, vol. 28, pp. 229–289, 1965.
[58] M. Versavel, G. A. Orban, and L. Lagae, "Responses of visual cortical neurons to curved stimuli and chevrons," *Vis. Res.*, vol. 30, pp. 235–248, 1990.
[59] E. Peterhans and R. von der Heydt, "Elements of form perception in monkey prestriate cortex," in *Representations of Vision. Trends and Tacit Assumptions*, A. Gorea, Y. Fregnac, Z. Kapoulis, and J. Findlay, Eds. Cambridge, U.K.: Cambridge Univ. Press, 1991, pp. 111–124.
[60] R. Baumann, R. van der Zwan, and E. Peterhans, "Figure-ground segregation at contours," *Eur. J. Neurosci.*, vol. 9, pp. 1290–1303, 1997.
[61] B. Heider, V. Meskenaite, and E. Peterhans, "Anatomy and physiology of a neural mechanism defining depth order and contrast polarity at illusory contours," *Eur. J. Neurosci.*, vol. 12, pp. 4117–4130, 2000.
[62] E. Peterhans and F. Heitger, "Simulation of neural responses defining depth order and contrast polarity at illusory contours in monkey area V2," *J. Comput. Neurosci.*, vol. 10, no. 2, pp. 195–211, 2001.
[63] R. von der Heydt, E. Peterhans, and M. R. Dürsteler, "Grating cells in monkey visual cortex: coding texture," in *Channels in the Visual Nervous System: Neurophysiology, Psychophysics and Models*, B. Blum, Ed. London, U.K.: Freund, 1991, pp. 53–73.
[64] ——, "Periodic-pattern-selective cells in monkey visual cortex," *J. Neurosci.*, vol. 12, pp. 1416–1434, 1992.
[65] G. Rizzolatti and R. Camarda, "Inhibition of visual responses of single units in the cat visual area of the lateral suprasylvian gyrus (Clare-Bishop area) by the introduction of a second visual stimulus," *Brain Res.*, vol. 88, no. 2, pp. 357–361, 1975.
[66] J. I. Nelson and B. J. Frost, "Orientation-selective inhibition from beyond the classic visual receptive field," *Brain Res.*, vol. 139, pp. 359–365, 1978.
[67] J. J. Knierim and D. C. van Essen, "Neuronal responses to static texture patterns in area V1 of the alert macaque monkey," *J. Neurophysiol.*, vol. 67, pp. 961–980, 1992.
[68] H. E. Jones, K. L. Grieve, W. Wang, and A. M. Sillito, "Surround suppression in primate V1," *J. Neurophysiol.*, vol. 86, no. 10, pp. 2011–2028, 2001.
[69] C. Blakemore and E. A. Tobin, "Lateral inhibition between orientation detectors in the cat's visual cortex," *Exp. Brain Res.*, vol. 15, pp. 439–440, 1972.
[70] E. De Yoe, J. Knierim, D. Sagi, B. Juilesz, and D. van Essen, "Single unit responses to static and dynamic texture patterns in macaque V2 and V1 cortex (abstract)," *Invest. Ophtalmol. Vis. Sci.*, vol. 27, no. Suppl., p. 18, 1986.
[71] W. Fries, K. Albus, and O. D. Creutzfeld, "Effects of interacting visual patterns on single cell responses in cat's striate cortex," *Vis. Res.*, vol. 17, pp. 1001–1008, 1977.
[72] A. Grinvald, D. Ts'o, R. D. Frostig, E. Lieke, A. Arieli, and R. Hildesheim, "Optical imaging of neuronal activity in the visual cortex," in *Neural Mechanisms of Visual Perception*, D. M.-K. Lam and C. Gilbert, Eds. Woodlands, TX: Portfolio, 1989, pp. 117–136.
[73] L. Maffei and A. Fiorentini, "The unresponsive regions of visual cortical receptive fields," *Vis. Res.*, vol. 16, pp. 1131–1139, 1976.
[74] J. R. Cavanaugh, W. Bair, and J. A. Movshon, "Orientation-selective setting of contrast gain by the surrounds of macaque striate cortex neurons," *Neurosci. Abstr.*, vol. 23, p. 227.2, 1997.
[75] P. H. Schiller, B. L. Finlay, and S. F. Volman, "Quantitative studies of single-cell properties in monkey striate cortex. III. Spatial frequencies," *J. Neurophysiol.*, vol. 39, pp. 1334–1351, 1976.
[76] N. Petkov and P. Kruizinga, "Computational models of visual neurons specialised in the detection of periodic and aperiodic oriented visual stimuli: bar and grating cells," *Biol. Cybern.*, vol. 76, no. 2, pp. 83–96, 1997.
[77] C. Blakemore, R. H. S. Carpenter, and M. A. Georgeson, "Lateral inhibition between orientation detectors in the human visual system," *Nature*, vol. 228, pp. 37–39, 1970.
[78] J. A. Solomon and D. G. Pelli, "The visual filter mediating letter identification," *Nature*, vol. 369, pp. 395–397, 1994.
[79] N. Petkov and M. A. Westenberg, "Suppression of contour perception by band-limited noise and its relation to nonclassical receptive field inhibition," *Biol. Cybern.*, vol. 88, pp. 236–246, 2003.
[80] A. Galli and A. Zama, "Untersuchungen über die Wahrnehmung ebener geometrischer Figuren, die ganz oder teilweise von anderen geometrischen Figuren verdeckt sind," *Zeitschrift für Psychologie*, vol. 123, pp. 308–348, 1931.
[81] S. Belongie, J. Malik, and J. Puzicha, "Shape matching and object recognition using shape contexts," *IEEE Trans. Pattern Anal. Machine Intell.*, vol. 24, no. 4, pp. 509–522, 2002.
[82] C. Grigorescu and N. Petkov, "Distance sets for shape filters and shape recognition," *IEEE Trans. Image Processing*, to be published.
[83] J. G. Daugman, "Uncertainty relation for resolution in space, spatial frequency, and orientation optimized by two-dimensional visual cortical filters," *J. Opt. Soc. Amer. A*, vol. 2, no. 7, pp. 1160–1169, July 1985.
[84] P. Kruizinga and N. Petkov, "Nonlinear operator for oriented texture," *IEEE Trans. Image Processing*, vol. 8, pp. 1395–1407, Oct. 1999.
[85] S. E. Grigorescu, N. Petkov, and P. Kruizinga, "Comparison of texture features based on Gabor filters," *IEEE Trans. Image Processing*, vol. 11, pp. 1160–1167, Oct. 2002.
[86] H. C. Nothdurft, J. L. Gallant, and D. C. van Essen, "Response modulation by texture surround in primate area V1: correlates of "popout" under anesthesia," *Vis. Neurosci.*, vol. 16, pp. 15–34, 1999.
[87] M. Sonka, V. Hlavac, and R. Boyle, *Image Processing, Analysis, and Machine Vision*. Pacific Grove, CA: Brooks/Cole, 1999.
[88] M. Heath, S. Sarkar, T. Sanocki, and K. Bowyer, "A robust visual method for assessing the relative performance of edge-detection algorithms," *IEEE Trans. Pattern Anal. Machine Intell.*, vol. 19, pp. 1338–1359, Dec. 1997.
[89] Y. T. Zhou, V. Venkateshwar, and R. Chellappa, "Edge detection and linear feature extraction using a 2-D random field model," *IEEE Trans. Pattern Anal. Machine Intell.*, vol. 11, pp. 84–95, 1989.
[90] L. Kitchen and A. Rosenfeld, "Edge evaluation using local edge coherence," *IEEE Trans. Syst., Man, Cybern.*, vol. 11, no. 9, pp. 597–605, 1981.
[91] M. Shin, D. Goldgof, and K. W. Bowyer, "An objective comparison methodology of edge detection algorithms for structure from motion task," in *Empirical Evaluation Techniques in Computer Vision*. New York: IEEE Press, 1998, pp. 235–254.
[92] M. C. Shin, K. W. Bowyer, and D. B. Goldgof, "Comparison of edge detectors through use in an object recognition task," *Comput. Vis. Image Understand.*, vol. 84, no. 1, pp. 160–178, 2001.
[93] Y. J. Zhang, "A survey on evaluation methods for image segmentation," *Pattern Recognit.*, vol. 29, no. 8, pp. 1335–1346, 1996.
[94] E. P. Simoncelli and O. Schwartz, "Modeling surround suppression in V1 neurons with a statistically-derived normalization model," in *Advances in Neural Information Processing Systems 11*, M. S. Kearns, S. A. Solla, and D. A. Cohn, Eds. Cambridge, MA: MIT Press, 1999, pp. 153–159.
[95] N. Petkov, P. Kruizinga, and T. Lourens, "Lateral inhibition in cortical filters," in *Proc. Int. Conf. on Digital Signal Processing*, Nicosia, Cyprus, July 14–16, 1993, pp. 122–129.
[96] ——, "Orientation competition in cortical filters—an application to face recognition," in *Computing Science in The Netherlands 1993*. Amsterdam, The Netherlands: Stichting Mathematisch Centrum, 1993, pp. 285–296.
[97] N. Petkov and T. Lourens, "Interacting cortical filters for object recognition," in *Proc. Asian Conf. Computer Vision*, Osaka, Japan, Nov. 23–25, 1993, pp. 583–586.
[98] N. Petkov and P. Kruizinga, "Perception of form and texture through complementary bar and grating cell channels," *Perception*, vol. 29, p. 60c, 2000.

Cosmin Grigorescu (S'98) received the Dipl.Eng. degree in 1995 and the M.S. degree in 1996 in computer science from Politehnica University of Bucharest, Romania. Since 1998, he has been pursuing the Ph.D. degree in the Department of Computing Science, University of Groningen, The Netherlands.

From 1996 to 1998, he taught and performed research at the Control and Computer Faculty, Politehnica University of Bucharest. His areas of research are image processing, computer vision and pattern recognition, with emphasis on models inspired from human vision.

Nicolai Petkov is Scientific Director of the Institute of Mathematics and Computing Science, University of Groningen, The Netherlands, where he holds the Chair of Parallel Computing and Intelligent Systems. He is author of two books and 90 scientific publications. His current research interests are in the area of computer simulations of the visual system, making links between computer vision, neurophysiology, psychophysics, and arts.

Michel A. Westenberg received the M.Sc. degree in computing science from the University of Groningen, The Netherlands, in 1996. In 2001, he received the Ph.D. degree in mathematics and natural sciences from the same university.

His current research interests are in the area of computer vision and scientific visualization.